

# Field-angle dependence of magnetoresistance in $\text{UTe}_2$

Jun Ishizuka<sup>1</sup> and Youichi Yanase<sup>2</sup>

<sup>1</sup>*Faculty of Engineering, Niigata University, Ikarashi, Niigata 950-2181, Japan*

<sup>2</sup>*Department of Physics, Graduate School of Science, Kyoto University, Kyoto 606-8502, Japan*

(Dated: March 19, 2026)

We theoretically study angle-resolved magnetoresistance under rotated magnetic field in the normal state of a spin-triplet superconductor  $\text{UTe}_2$ . The Wannier model derived from a GGA+ $U$  calculation shows quasi-two-dimensional Fermi surfaces with warping in the  $k_z$  direction, consistent with quantum oscillation measurements in the high magnetic field regime. Solving the semiclassical Boltzmann equation, we show that the Fermi surface geometry gives rise to oscillations in the magnetoresistance when the field is tilted from the  $c$  axis toward the  $a$  or  $b$  axis. By assuming a band-dependent relaxation time, the calculated angle-resolved magnetoresistance is in good agreement with the recent transport experiment. This is direct evidence for the warped Fermi surface revealed by ordinary intraband transport. It suggests that the hole band with long relaxation time dominates electron transport. The field angle dependence of the Hall resistivity is calculated for further experimental verification.

## I. INTRODUCTION

Superconductivity in the heavy fermion compound  $\text{UTe}_2$  [1–3] has attracted intense attention due to their exotic properties [4–17], including the multicomponent spin-triplet superconductivity [18–24] and the potential of topological superconductivity [25–30]. Topological superconductors accompanied by Majorana fermion excitations hold considerable promise for quantum computing applications [31–33]. Evidence supporting spin-triplet pairing in  $\text{UTe}_2$  includes extraordinarily high upper critical fields [1], reentrant superconductivity near metamagnetic transitions [4, 5], and slight decreases in spin susceptibility below the superconducting transition temperature  $T_c$  [34–39]. However, despite substantial efforts by theories and experiments [40–63], the electronic structure, pairing mechanisms, and symmetry of superconductivity remain unsolved.

Intensive studies have been dedicated to the identification of the Fermi surface (FS) [64–70], which is crucial to a comprehensive understanding of exotic phenomena in  $\text{UTe}_2$ . First-principles calculations have predicted a wide range of underlying band structures [2]. Although the band structures far below the Fermi level are consistent between naive band calculations and angle-resolved photoemission spectroscopy (ARPES) measurements [64], first-principles calculations predict Kondo-insulating-like bands, which contradict the metallic behavior of  $\text{UTe}_2$ . Later, the GGA+ $U$  calculation and the density functional theory combined with dynamical mean field theory (DFT+DMFT) find quasi-two-dimensional (2D) hole and electron FSs in agreement with ARPES [25, 46, 65]. High-quality single crystals with  $T_c \sim 2.1$  K were recently synthesized [71, 72], and thereby the de Haas–van Alphen (dHvA) effect has been observed. The angular dependence of the dHvA frequencies revealed the warping of cylindrical 2D FSs in good agreement with the GGA+ $U$  calculation [67]. The existence of three-dimensional (3D) FS was reported by Shubnikov-de Haas (SdH) oscillations [69] and implied by  $c$ -axis transport [73]. Several theoretical studies also predicted a small 3D FS centered at the  $\Gamma$ -point [64, 74, 75]. However, such a 3D FS was not detected in recent dHvA and SdH measurements [76].

Quantum interference oscillations (QIOs) in magnetoresistance and magnetoconductance are a useful tool to investigate the bulk electronic structure [77, 78]. Unlike quantum oscillations from the dHvA and SdH effects, the QIOs are attributed to the semiclassical orbital motions of quasiparticles connecting separate FS sections. Therefore, QIOs and quantum oscillations can be complementary probes of the FS topology. In  $\text{UTe}_2$ , the appearance of QIOs for magnetic fields along the  $a$  and  $c$  axes has been reported [77, 78].

Angle-resolved magnetoresistance is also informative for detecting the FS topology [79–81]. A recent experiment of  $\text{UTe}_2$  shows a monotonic increase of the  $c$ -axis resistivity  $\rho_{zz}$  when the magnetic field is rotated from the  $c$  axis to the  $b$  axis, while it shows a nonmonotonic behavior with dips when the field is rotated toward the  $a$  axis [82]. These behaviors of the angle-dependent magnetoresistance may be attributed to the warping of FSs. However, an explicit calculation has been lacking.

Inspired by the experimental transport studies, we investigate the angle-resolved magnetoresistance with a microscopic Wannier model derived from the first-principles band structure calculations with the warped 2D FSs. By introducing the band dependence of the relaxation time, which is compatible with the antiferromagnetic fluctuation with the wave vector  $\mathbf{q} \sim (0, \pi, 0)$  observed in the neutron scattering experiments [12, 13], it is shown that the magnetic field angular dependence of resistivity reported in Ref. 82 is explained by the majority contribution from the warped hole FS with small Fermi velocity. This is direct evidence for the warped FSs revealed by ordinary intraband transport.

## II. METHOD

To calculate angle-resolved magnetoresistance, the electronic structure is described by density functional theory using the Wien2k code [83]. To include the correlation effects on uranium atoms, we adopt a GGA+ $U$  method implemented in Wien2k. We construct a Wannier model using Wannier90 [84] through the wien2wannier interface [85] for  $U = 2.0$  eV. It is beneficial to reproduce the electronic states near the Fermi en-

ergy with a small number of Wannier orbitals to reduce a calculation time. Thus, we set projectors from the Bloch states to the Wannier functions as  $5f_{z^3}$  and  $6d_{3z^2-r^2}$  orbitals on the two U sites and  $5p_y$  orbitals on the two Te(2) sites [Fig. 1(a)] with spin degree of freedom, resulting in a 12-band model. We perform a 100-times Wannierization with  $12 \times 12 \times 12$   $\mathbf{k}$ -points. For comparison, we also constructed a 72-band Wannier model.

The conductivity/resistivity tensor is calculated using the Boltzmann equation with the semiclassical and relaxation time approximation as implemented in the WannierTools package [81, 86]. Here, we briefly look at the formulas [87]. The conductivity tensor with the magnetic field  $\mathbf{B}$  is given by

$$\sigma_{ij}^n(\mathbf{B}) = \frac{e^2}{4\pi^3} \int d\mathbf{k} \tau_n v_i^n(\mathbf{k}) \bar{v}_j^n(\mathbf{k}) \left( -\frac{\partial f}{\partial \varepsilon} \right)_{\varepsilon=\varepsilon_n(\mathbf{k})}, \quad (1)$$

where  $\tau_n$  is the relaxation time at band  $n$ ,  $f$  is the Fermi-Dirac distribution function,  $v_i^n(\mathbf{k})$  is the velocity for  $i = x, y, z$  direction, defined by  $\mathbf{v}^n(\mathbf{k}) = \nabla_{\mathbf{k}} \varepsilon_n(\mathbf{k}) / \hbar$ . In the above formula,  $\bar{v}_i^n(\mathbf{k})$  is the weighted average of velocity over the past history of the electron orbital motion

$$\bar{\mathbf{v}}^n(\mathbf{k}) = \int_{-\infty}^0 \frac{dt}{\tau_n} e^{\frac{t}{\tau_n}} \mathbf{v}^n(\mathbf{k}_n(t)), \quad (2)$$

with the time evolution of the wave vector  $\mathbf{k}_n(t)$ ,

$$\frac{d\mathbf{k}_n(t)}{dt} = -\frac{e}{\hbar} \mathbf{v}^n(\mathbf{k}(t)) \times \mathbf{B}. \quad (3)$$

The Runge-Kutta method is adopted to solve Eq. (3). The total conductivity tensor is obtained by summing the contributions of the bands,  $\hat{\sigma}(\mathbf{B}) = \sum_n \hat{\sigma}^n(\mathbf{B})$ . The resistivity tensor is given by the inverse of the conductivity tensor  $\hat{\rho}(\mathbf{B}) = [\sum_n \hat{\sigma}^n(\mathbf{B})]^{-1}$ . Note that in the semiclassical approximation, interband effects such as QIOs due to magnetic breakdown are neglected. We also assume that the FSs are not affected by the Zeeman field. In the numerical calculations,  $27 \times 27 \times 27$   $\mathbf{k}$ -points are used.

### III. RESULT

#### A. Electronic structure

Figure 1(b) shows the band structure obtained in the DFT+ $U$  calculation for  $U = 2.0$  eV and that of the 12-band Wannier model. We see that the Wannier model reproduces the low-energy states near the Fermi energy. The FSs of the Wannier model are illustrated in Fig. 1(c), which shows two rectangular FSs. The quasi-2D electron sheet shows warping near the  $k_y = \pm\pi/2$  plane around the  $S$ -point. A large Fermi velocity is obtained in the warped region, while the Fermi velocity is small in the flat plane around  $k_x \sim \pm\pi/2$ . These features are attributed to the one-dimensional (1D) dispersion of the  $d_{3z^2-r^2}$  orbitals along the  $k_x$  direction and the 1D dispersion of the  $p_y$  orbitals along the  $k_y$  direction. As a consequence of finite hybridization between these bands and U  $5f$ -electrons, the electron FS shows a shape similar to a warped

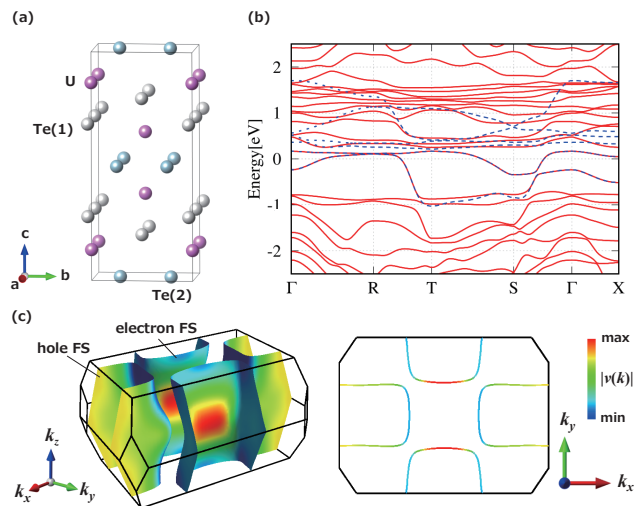


FIG. 1. (a) Crystal structure of  $\text{UTe}_2$ . (b) Band structure of the DFT+ $U$  calculation for  $U = 2.0$  eV (solid lines) and the 12-band Wannier model (dashed lines) along the high symmetry lines. (c) Left: Fermi surfaces of the 12-band Wannier model. Right: 2D cut on the  $k_z = 0$  plane. The magnitude of Fermi velocity is indicated by color.

rectangular tube with different velocity between the  $k_x$  and  $k_y$  axes. The hole FS sheet can be understood in a similar way. However, unlike the electron FS sheet, the warping appears around the  $k_x \sim \pm\pi/2$  plane, and the Fermi velocity is small there.

The band structure of the 12-band Wannier model is in good agreement with the 72-band Wannier model not only for the shape of the FSs but also for the Fermi velocity on the FSs. Therefore, the 12-band Wannier model is a reasonable basis for the theoretical study of intraband transport. The FSs are consistent with the quantum oscillation experiments [67, 70], and ARPES has also observed quasi-2D FSs [65].

#### B. Magnetoresistance with band-independent relaxation time

The resistivity tensor as a function of the magnetic field is shown in Figs. 2(a)-2(c), where we set the field angle  $\mathbf{B} \parallel c$  ( $\theta = \phi = 0$  deg) and the band-independent relaxation time  $\tau_h = \tau_e = 1.0$  ps. In the following, we define the field angle  $\theta, \phi$  as the polar and azimuthal angles, respectively. The initial increase in diagonal resistivity as a function of the magnetic field  $B$  follows a quadratic dependence. We see the anisotropy  $\rho_{yy} < \rho_{xx}$  at  $B = 0$  T for temperatures  $30 \text{ K} < T < 330 \text{ K}$ , contrary to Ref. 73 reporting  $\rho_{xx} < \rho_{yy}$ , but consistent with a recent study using FIB microstructures that found  $\rho_{yy} < \rho_{xx}$  [59]. The anisotropy  $\rho_{xx} < \rho_{yy}$  will be obtained by introducing a  $\mathbf{k}$ -dependent relaxation time as shown in Ref. 70. However, this is not within the scope of the present study and will not be further discussed because the angle-resolved magnetoresistance is mainly determined by the warped part of FSs and expected to be insensitive to this  $\mathbf{k}$ -dependence. The ratio

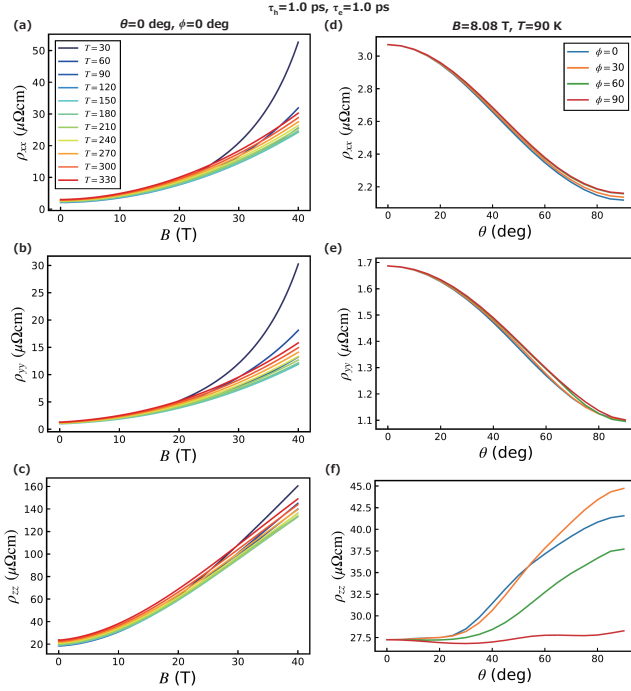


FIG. 2. (a)-(c) Magnetic field  $B$  dependence of diagonal resistivity, namely, the magnetoresistance, for the field angle  $\theta = \phi = 0$  deg. The temperature is varied from 30 K to 330 K. (d)-(f) Field angle  $\theta$  dependence of resistivity at various angles  $\phi$  for  $B = 8.08$  T and  $T = 90$  K. A band-independent relaxation time  $\tau_h = \tau_e = 1.0$  ps is assumed.

$\rho_{zz}/\rho_{xx} = 8.6$  at  $B = 0$  T and  $T = 30$  K is of the same order as the experimental value [73].

The resistivity tensor as a function of the field angle  $\theta$  is shown in Figs. 2(d)-2(f) where  $B = 8.08$  T and  $T = 90$  K. The in-plane resistivity  $\rho_{xx}$  and  $\rho_{yy}$  are monotonically suppressed by increasing angle  $\theta$  and are almost independent of  $\phi$ . In contrast, we see that the  $c$ -axis resistivity  $\rho_{zz}$  shows a nonmonotonic field angle  $\theta$  dependence [Fig. 2(f)]:  $\rho_{zz}$  increases monotonically when the magnetic field is rotated from the  $c$  axis to the  $a$  axis ( $\phi = 0$  deg), but weakly oscillates when rotated toward the  $b$  axis ( $\phi = 90$  deg). However, these behaviors of  $\rho_{zz}$  are qualitatively contrary to the experimental results [82].

To resolve the discrepancy with the experiment, we discuss the reason behind these behaviors by studying the band-resolved resistivity and conductivity. The total conductivity is given by the summation of the hole and electron band components,  $\sigma_{ij} = 2(\sigma_{ij}^h + \sigma_{ij}^e)$ . Here, factor 2 comes from the spin degree of freedom. When we consider only the hole band and neglect  $\sigma_{ij}^e$ , we obtain the band-resolved resistivity  $\hat{\rho}^h(\mathbf{B}) = [\hat{\sigma}^h(\mathbf{B})]^{-1}$  in Fig. 3(a), which clearly exhibits a trend opposite to Fig. 2(f). At  $\phi = 0$  deg, the band-resolved  $\rho_{zz}^h$  for the hole band oscillates with respect to  $\theta$ . When  $\phi$  is increased, the resistivity increases. In contrast, the band-resolved  $\rho_{zz}^e$  for the electron band, which is obtained by neglecting  $\sigma_{ij}^h$ , shows similar behaviors to the total resistivity and weakly oscillates at  $\phi = 90$  deg.

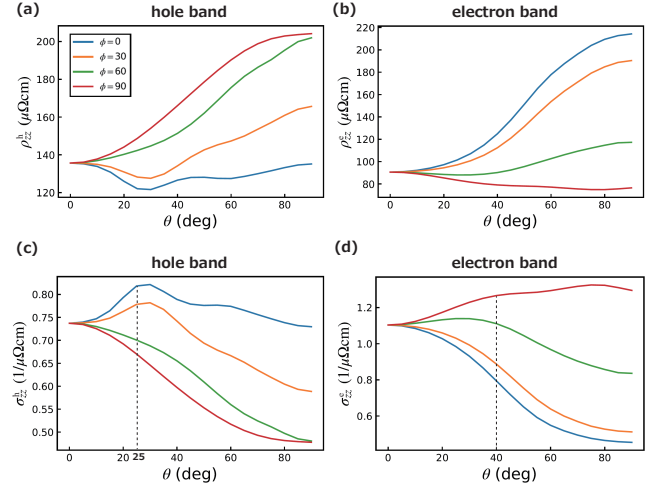


FIG. 3. Field angle  $\theta$  dependence of band-resolved resistivity [(a), (b)] and conductivity [(c), (d)]. We set the same parameters as Fig. 2(f),  $B = 8.08$  T,  $T = 90$  K, and illustrate the results for each field angle  $\phi$  by the same color. Dashed lines in (c) and (d) depict the angles  $\theta$  adopted in Figs. 4(b) and 4(d), respectively.

The above analysis indicates that the field angle dependence of the total resistivity  $\rho_{zz}$  is dominated by the electron band component  $\sigma_{zz}^e$ , when the relaxation time is independent of the bands. In this case, the calculation result of the angle-resolved magnetoresistance [Fig. 2(f)] is qualitatively incompatible with the experiment [82]. The analysis of the band-resolved resistivity naturally leads to an idea. When the relaxation time of the hole band is longer than that of the electron band, the transport is dominated by the hole band, and the field angle dependence of magnetoresistance  $\rho_{zz}$  can become consistent with the experiment. We examine this idea in the next subsection.

To gain an intuitive understanding of the magnetoresistance, here we discuss the origin of the field angle dependence. The field angle dependence of  $\sigma_{zz}^{e,h}$  can be understood by considering the semiclassical trajectories of the carrier and  $\bar{v}_z(\mathbf{k})$ . Figures 4(a) and 4(b) show the cross sections of the hole FS in the  $k_x$ - $k_z$  plane at  $k_y = 0$ . Typical orbits of hole carriers in the magnetic field oriented along the  $c$  axis ( $\theta = \phi = 0$  deg) [Fig. 4(a)] and  $\theta = 25$  deg and  $\phi = 0$  deg [Fig. 4(b)] are labeled by (i)-(iv), where the band-resolved conductivity  $\sigma_{zz}^h$  shows a minimum and maximum, respectively. In the hole orbit (i), the velocity  $v(\mathbf{k})$  has only in-plane components, and therefore this orbit does not contribute to the  $c$ -axis conductivity  $\sigma_{zz}^h$ . In the other hole orbit (ii),  $v_z(\mathbf{k})$  has a different sign on the opposite sides of the warped FS. This results in the cancellation of  $\bar{v}_z(\mathbf{k})$  and decreases  $\sigma_{zz}^h$ . When the magnetic field  $\mathbf{B}$  is rotated toward the  $a$  axis, the orbit (i) changes to the orbit (iii) and encounters an extremum of the FS at  $\theta = 25$  deg. At this angle, the orbit (iii) again gives no contribution to  $\sigma_{zz}^h$ , similar to the orbit (i). However, in the hole orbit (iv), the trajectory avoids cancellation in contrast to the orbit (ii), resulting in a net increase in  $\sigma_{zz}^h$ . By further tilting the mag-

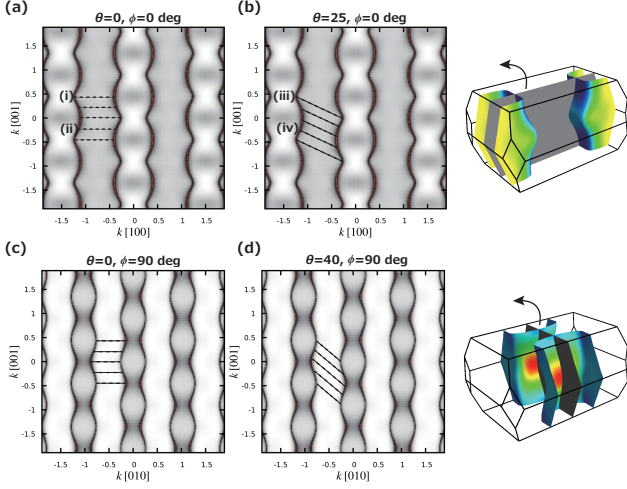


FIG. 4. (a), (b) Cross sections of the hole FS in the  $k_x$ - $k_z$  plane at  $k_y = 0$ . Typical orbits of the hole carriers in the magnetic field oriented along the angle (a)  $\theta = \phi = 0$  deg and (b)  $\theta = 25$  deg and  $\phi = 0$  deg are labeled by (i)-(iv). (c), (d) Cross sections of the electron FS in the  $k_y$ - $k_z$  plane at  $k_x = 0$ . Orbits of the electron carriers are illustrated by dashed lines.

netic field, the trajectories again pass through  $\mathbf{k}$ -points with a sign change of  $v_z(\mathbf{k})$  as in the case of  $\theta = \phi = 0$  because of the periodicity of the reciprocal lattice, implying a decrease of  $\sigma_{zz}^h$ . This is a mechanism of the field angular oscillation of the conductivity due to the warping of the FS. We encounter the same situation for the electron FS when the magnetic field is tilted from the  $c$  axis to the  $b$  axis [Figs. 4(c) and 4(d)]. Because the warping planes are orthogonal between the hole and electron FSs, the field angle dependencies of  $\sigma_{zz}^h$  and  $\sigma_{zz}^e$  and the corresponding magnetoresistance show qualitatively different behaviors.

### C. Magnetoresistance with band-dependent relaxation time

In the previous section, we assumed band-independent relaxation time and showed that the field angle dependence of magnetoresistance is inconsistent with the experiment for  $\text{UTe}_2$  [82] because the contribution from the electron band is dominant. As shown in Figs. 3(c) and 3(d), the hole band component of the conductivity is qualitatively different from the electron band component, and the corresponding resistivity in Fig. 3(a) shows the field angle dependence in agreement with the experimental results [82]. Therefore, we consider the band-dependent relaxation time and assume  $\tau_h > \tau_e$ . A shorter relaxation time of the electron band is consistent with the dHvA experiment, which suggests  $\tau_h > \tau_e$  since the dHvA amplitude of the electron band is much smaller than that of the hole band [67].

The microscopic origin of the band-dependent relaxation time could be attributed to magnetic fluctuations. In  $\text{UTe}_2$ , antiferromagnetic fluctuation with the wave vector  $\mathbf{q} \sim (0, \pi, 0)$  has been observed in neutron scattering experiments [12, 13].

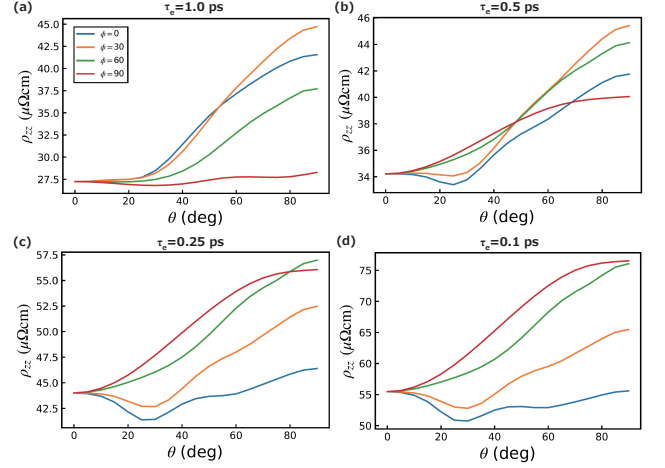


FIG. 5. (a)-(d) Field angle  $\theta$  dependence of the  $c$ -axis resistivity with the band-dependent relaxation time. We fix  $\tau_h = 1.0$  ps and vary  $\tau_e$  from (a) 1.0 ps to (d) 0.1 ps. The other parameters,  $B = 8.08$  T and  $T = 90$  K, are the same as Fig. 2(f).

The self-energy correction from this magnetic fluctuation yields a strong quasiparticle damping on the FSs with a nesting vector  $\mathbf{q} \sim (0, \pi, 0)$ . Thus, the relaxation time is expected to be short on the FSs around the  $k_y = \pm\pi/2$  plane, including the warping part of the electron FS. For simplicity, we neglect the momentum dependence of the relaxation time  $\tau_n(\mathbf{k})$  on each band. This is justified for the following discussions because the magnetoresistance is mainly determined by the warped parts of the FSs.

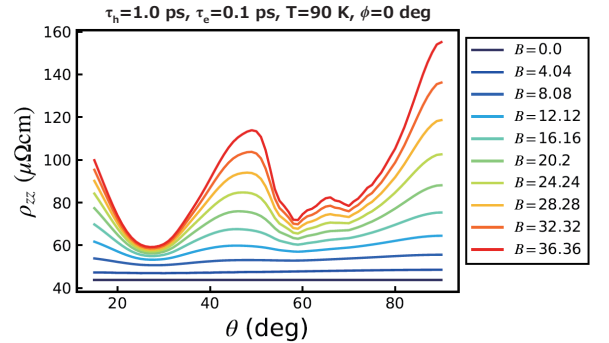


FIG. 6. Field angle  $\theta$  dependence of the  $c$ -axis resistivity for  $T = 90$  K,  $\tau_h = 1.0$  ps,  $\tau_e = 0.1$  ps, and  $\phi = 0$  deg. The magnetic field is increased from  $B = 0$  T to  $B = 36.36$  T from the bottom to the top.

In Fig. 5, we show the  $\theta$  dependence of the total resistivity  $\rho_{zz}$  for several relaxation times  $\tau_e$  of the electron band. The relaxation time of the hole band is fixed to  $\tau_h = 1.0$  ps, and we assume  $B = 8.08$  T and  $T = 90$  K as in Fig. 3. The results for  $\tau_e = 0.25$  and 0.1 ps appear to be consistent with the experiment [82]. We see in Figs. 5(c) and 5(d) that the resistivity  $\rho_{zz}$  is gradually suppressed as the angle  $\phi$  decreases. For  $\phi = 0$

deg, the resistivity oscillates as a function of  $\theta$ , and a first minimum appears at  $\theta_1 = 25\text{--}30$  deg, in good agreement with the experimental result  $\theta_1^{\text{exp}} = 30$  deg. We find the second maximum at  $\theta_2 = 45\text{--}50$  deg, which is also consistent with the experimental observation  $\theta_2^{\text{exp}} = 48$  deg. Figure 5 does not show a distinguished peak at higher  $\theta$ , although peaks at  $\theta_3^{\text{exp}} = 65$  deg and  $\theta_4^{\text{exp}} = 72$  deg are experimentally observed. The discrepancy is partially solved, when we increase the magnetic field  $B$ . An additional peak appears at  $\theta_3 = 65$  deg for  $B > 20$  T (Fig. 6), consistent with the experiment. Thus, the field angle dependence of the resistivity  $\rho_{zz}$ , including the oscillation in the high angle region, is reproduced and attributed to the properties of the hole FS.

Due to the limitation on the number of  $\mathbf{k}$ -points, the magnetoresistance has been calculated at the temperature  $T = 90$  K higher than the experimental value  $T \sim 1.5$  K [82]. We have confirmed that the main results in this paper are unchanged in the calculations at  $T = 30$  K. Thus, the obtained results of the field angle dependence are expected to be robust in lowering the temperature  $T$ .

#### D. Off-diagonal transport

Next, we address the field angle dependence of the transverse (Hall) resistivity. From the symmetry constraint, the Hall resistivity  $\rho_{ij}$  vanishes when the magnetic field is aligned with either the  $i$  or  $j$  axis. The Hall resistivity in the isotropic 2D model with hole and electron carriers is given by [81]

$$\rho_{xy} = -\frac{1}{e} \frac{(n_h \mu_h^2 - n_e \mu_e^2) B + \mu_e^2 \mu_h^2 (n_h - n_e) B^3}{(n_h \mu_h + n_e \mu_e)^2 + (n_e - n_h)^2 \mu_e^2 \mu_h^2 B^2}, \quad (4)$$

for  $\mathbf{B} = B\hat{z}$ , indicating that  $\rho_{xy} = 0$  if  $n_h = n_e$  and  $\mu_h = \mu_e$ . Although  $\text{UTe}_2$  is a compensated metal, the Hall conductivity becomes finite because of the anisotropic mobility in the orthorhombic structure.

We present the Hall resistivity obtained by considering either the hole or electron band in Fig. 7. The signs of the band-resolved resistivity tensor can be explained by considering  $v_i(\mathbf{k})$  and  $\bar{v}_j(\mathbf{k})$  in terms of the Boltzmann equation (Fig. 8). The Hall resistivity  $\rho_{xy}^{\text{e,h}}$  and  $\rho_{zx}^{\text{e,h}}$  follow the sign expected from a simple formula Eq. (4): The electron (hole) band gives positive (negative) Hall resistivity. However, we obtain a counterintuitive result for  $\rho_{yz}^{\text{e}} \geq 0$  at  $\phi = 90$  deg [Fig. 7(b)] and  $\rho_{yz}^{\text{e}} \leq 0$  [Fig. 7(e)], which is given by

$$\rho_{yz}^n = -(\sigma_{xx}^n \sigma_{yz}^n - \sigma_{xz}^n \sigma_{yx}^n) / \det(\hat{\sigma}^n). \quad (5)$$

Note that we observe  $\rho_{yz}^{\text{e}} \leq 0$  in the almost whole parameter space ( $B = 0\text{--}40$  T,  $T = 30\text{--}300$  K,  $\theta = 0\text{--}90$  deg,  $\phi = 0\text{--}90$  deg). This is due to the curvature of the warped electron FS with a large velocity, as illustrated in Fig. 8(c). Because  $|v(\mathbf{k})|$  is large in the region (i), the  $\mathbf{k}$ -resolved Hall conductivity  $\sigma_{yz}^n(\mathbf{k}) \equiv \tau_n v_y^n(\mathbf{k}) \bar{v}_z^n(\mathbf{k}) \left( -\frac{\partial f}{\partial \varepsilon} \right)_{\varepsilon=\varepsilon_n(\mathbf{k})}$  in the region (i) is larger than in the region (ii). In Fig. 8(c), we see that the region (i) gives a positive  $\sigma_{yz}^{\text{e}}(\mathbf{k})$  as  $v_y^{\text{e}}(\mathbf{k}) \bar{v}_z^{\text{e}}(\mathbf{k}) > 0$ . Since the first term dominates in Eq. (5), we get  $\rho_{yz}^{\text{e}} \leq 0$ .

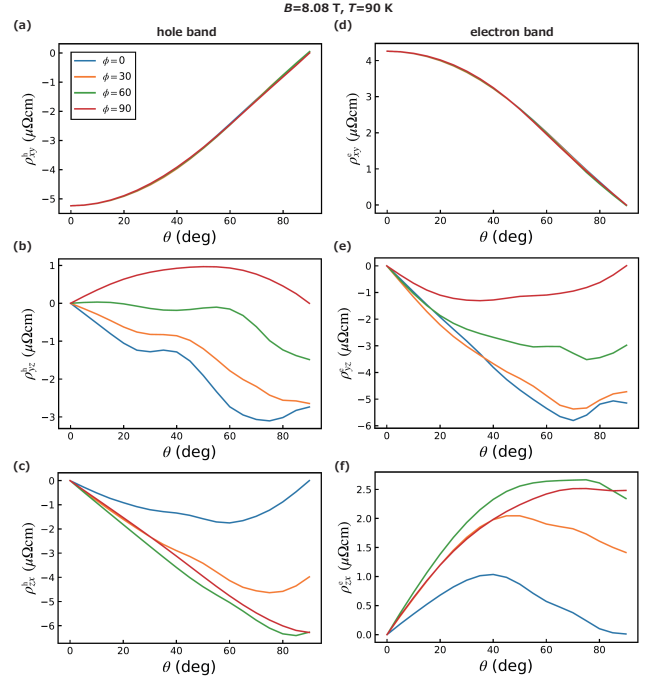


FIG. 7. Field angle  $\theta$  dependence of the band-resolved Hall resistivity for  $B = 8.08$  T,  $T = 90$  K,  $\tau_h = \tau_e = 1.0$  ps, and various field angles  $\phi$ . (a)–(c) [(d)–(f)] Only the hole (electron) band is taken into account.

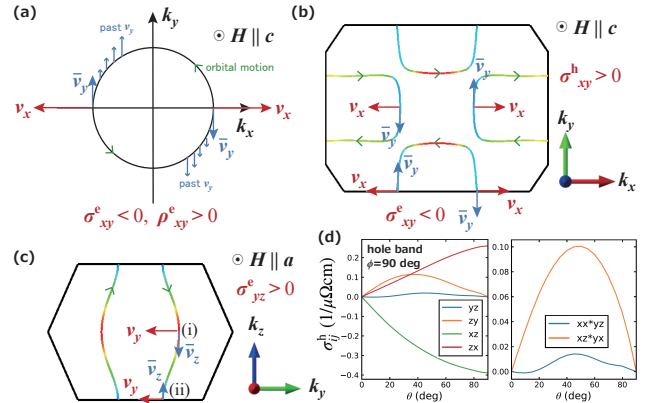


FIG. 8. (a) Schematic picture for the Hall conductivity and resistivity in the isotropic 2D free electron model. In the formula derived from the Boltzmann equation, Eq. (1),  $\bar{v}_y$  is calculated by integrating the transverse velocity  $v_y$  over the past history ( $t < 0$ ) with the weight factor  $e^{t/\tau_n}$ . Because  $v_x \bar{v}_y < 0$  at  $\mathbf{k} = (\pm k_F, 0)$  that give dominant contribution to  $\sigma_{xy}$ , we obtain  $\sigma_{xy}^{\text{e}} < 0$  and  $\rho_{xy}^{\text{e}} > 0$ , although a small positive contribution  $\sigma_{xy}^{\text{e}}(\mathbf{k}) > 0$  comes from the region  $k_x k_y > 0$ . (b) Schematic illustration for the Hall conductivity  $\sigma_{xy}^{\text{e,h}}$  in  $\text{UTe}_2$  under the magnetic field along the  $c$  axis. We can intuitively understand  $\sigma_{xy}^{\text{e}} < 0$   $\sigma_{xy}^{\text{h}} > 0$  as in the isotropic electron and hole models. (c) Schematic illustration for the Hall conductivity  $\sigma_{yz}^{\text{e}}$  due to the electron band under the magnetic field along the  $a$  axis. (d) Left: some components of Hall conductivity  $\sigma_{ij}^h$  in the hole band. Right:  $\sigma_{xx}^h \sigma_{yz}^h$  and  $\sigma_{xz}^h \sigma_{yx}^h$ . Field angle  $\theta$  dependence for  $B = 8.08$  T,  $T = 90$  K, and  $\phi = 90$  deg are plotted.

There is a different reason for the positive Hall resistivity in the hole band  $\rho_{yz}^h \geq 0$  at  $\phi = 90$  deg. We find a small Hall conductivity  $\sigma_{yz}^h$ , as shown in Fig. 8(d). This is because the hole FS is elongated along the  $k_x$  direction, and the Fermi velocity is small on the warped part of the FS. This is in contrast to the electron band, where the warped FS has a large velocity. In the hole band, because  $\sigma_{yz}^h$  is much smaller than  $\sigma_{xz}^h$ , the second term dominates in Eq. (5) [see right panel in Fig. 8(d)], and we have  $\rho_{yz}^h \geq 0$ .

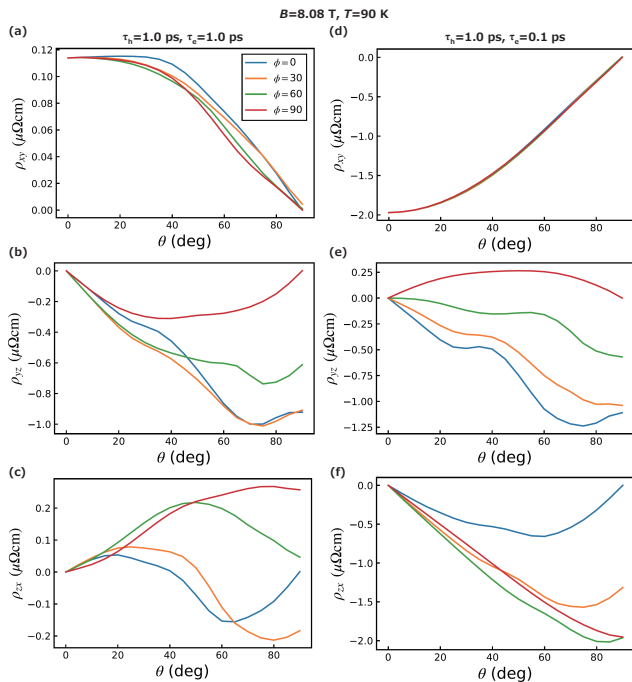


FIG. 9. Field angle  $\theta$  dependence of the Hall resistivity for  $B = 8.08$  T and  $T = 90$  K in each field angle  $\phi$ . (a)-(c) The results with band-independent relaxation time  $\tau_h = \tau_e = 1.0$  ps and (d)-(f) with band-dependent relaxation time  $\tau_h = 1.0$  ps and  $\tau_e = 0.1$  ps.

The field angular dependence of the total Hall resistivity is shown in Fig. 9, where we set  $\tau^e = 1.0$  or  $0.1$  ps. For  $\tau^e = 1.0$  ps, we see that the  $\theta$  dependence of  $\rho_{xy}$  [Fig. 9(a)] and  $\rho_{yz}$  [Fig. 9(b)] is similar to  $\rho_{xy}^e$  [Fig. 7(d)] and  $\rho_{yz}^e$  [Fig. 7(e)],

where transport is determined by the electron band. Similarly to the diagonal resistivity, these off-diagonal components of resistivity are dominated by the electron band when the relaxation time is independent of the band. In contrast,  $\rho_{zx}$  shows a complicated  $\theta$  dependence due to the contribution of the hole band. When we assume a short relaxation time  $\tau^e = 0.1$  of the electron band, as expected, all components of Hall resistivity [Figs. 9(d)-(f)] resemble the results for the hole band.

To our best knowledge, field angle dependence of off-diagonal transport in  $\text{UTe}_2$  has not been reported. Thus, we expect that future experimental studies of off-diagonal transport, compared with our calculation results, will provide further information on the FS and the quasiparticle's relaxation time.

#### IV. SUMMARY

We have investigated the magnetic field angular dependence of magnetoresistance in the normal state of the spin-triplet superconductor  $\text{UTe}_2$ . By applying the semiclassical Boltzmann equation to a 12-band Wannier model, we demonstrated that both the electron and hole bands contribute to the anisotropic magnetoresistance oscillations in the  $c$  axis transport with respect to the magnetic field angle. The calculated angular dependence of the magnetoresistance agrees with the experimental results when the relaxation time of the electron band is shorter than that of the hole band, suggesting the importance of the hole band in the electron transport. Electron correlation through magnetic fluctuations is expected to play an essential role in determining the band-dependent relaxation time. We also find nontrivial behaviors in the Hall resistivity, including a sign change. Experimental observation of this phenomenon would serve as a fingerprint of the FS topology.

#### ACKNOWLEDGMENTS

We appreciate helpful discussions with Motoi Kimata and Toni Helm. Some figures in this paper were created by using VESTA [88] and FermiSurfer [89]. This work was supported by JSPS KAKENHI (Grant Numbers JP22H01181, JP22H04933, JP23K17353, JP23K22452, JP24K21530, JP24H00007, JP25H01249, JP25K07223).

- 
- [1] S. Ran, C. Eckberg, Q.-P. Ding, Y. Furukawa, T. Metz, S. R. Saha, I.-L. Liu, M. Zic, H. Kim, J. Paglione, and N. P. Butch, Nearly ferromagnetic spin-triplet superconductivity, *Science* **365**, 684 (2019).
  - [2] D. Aoki, A. Nakamura, F. Honda, D. Li, Y. Homma, Y. Shimizu, Y. J. Sato, G. Knebel, J.-P. Brison, A. Pourret, D. Braithwaite, G. Lapertot, Q. Niu, M. Vališka, H. Harima, and J. Flouquet, Unconventional superconductivity in heavy fermion  $\text{ute}_2$ , *J. Phys. Soc. Jpn.* **88**, 043702 (2019).
  - [3] D. Aoki, J.-P. Brison, J. Flouquet, K. Ishida, G. Knebel, Y. Tokunaga, and Y. Yanase, Unconventional superconductivity in  $\text{ute}_2$ , *Journal of Physics: Condensed Matter* **34**, 243002 (2022).
  - [4] G. Knebel, W. Knafo, A. Pourret, Q. Niu, M. Vališka, D. Braithwaite, G. Lapertot, M. Nardone, A. Zitouni, S. Mishra, I. Sheikin, G. Seyfarth, J.-P. Brison, D. Aoki, and J. Flouquet, Field-reentrant superconductivity close to a metamagnetic transition in the heavy-fermion superconductor  $\text{ute}_2$ , *J. Phys. Soc. Jpn.* **88**, 063707 (2019).
  - [5] S. Ran, I.-L. Liu, Y. S. Eo, D. J. Campbell, P. M. Neves, W. T. Fuhrman, S. R. Saha, C. Eckberg, H. Kim, D. Graf, F. Balakirev, J. Singleton, J. Paglione, and N. P. Butch, Extreme magnetic field-boosted superconductivity, *Nat. Phys.* **15**, 1250 (2019).
  - [6] Y. Tokunaga, H. Sakai, S. Kambe, T. Hattori, N. Higa, G. Nakamine, S. Kitagawa, K. Ishida, A. Nakamura,

- Y. Shimizu, Y. Homma, D. Li, F. Honda, and D. Aoki, 125Te-nmr study on a single crystal of heavy fermion superconductor  $Ute_2$ , *J. Phys. Soc. Jpn.* **88**, 073701 (2019).
- [7] W. Knafo, M. Vališka, D. Braithwaite, G. Lapertot, G. Knebel, A. Pourret, J.-P. Brison, J. Flouquet, and D. Aoki, Magnetic-field-induced phenomena in the paramagnetic superconductor  $Ute_2$ , *J. Phys. Soc. Jpn.* **88**, 063705 (2019).
- [8] A. Miyake, Y. Shimizu, Y. J. Sato, D. Li, A. Nakamura, Y. Homma, F. Honda, J. Flouquet, M. Tokunaga, and D. Aoki, Metamagnetic transition in heavy fermion superconductor  $Ute_2$ , *J. Phys. Soc. Jpn.* **88**, 063706 (2019).
- [9] S. M. Thomas, F. B. Santos, M. H. Christensen, T. Asaba, F. Ronning, J. D. Thompson, E. D. Bauer, R. M. Fernandes, G. Fabbris, and P. F. S. Rosa, Evidence for a pressure-induced antiferromagnetic quantum critical point in intermediate-valence  $Ute_2$ , *Science Advances* **6**, 10.1126/sciadv.abc8709 (2020).
- [10] S. Bae, H. Kim, Y. S. Eo, S. Ran, I.-I. Liu, W. T. Fuhrman, J. Paglione, N. P. Butch, and S. M. Anlage, Anomalous normal fluid response in a chiral superconductor  $Ute_2$ , *Nature Communications* **12**, 2644 (2021).
- [11] S. Sundar, S. Gheidi, K. Akintola, A. M. Côté, S. R. Dunsiger, S. Ran, N. P. Butch, S. R. Saha, J. Paglione, and J. E. Sonier, Coexistence of ferromagnetic fluctuations and superconductivity in the actinide superconductor  $Ute_2$ , *Phys. Rev. B* **100**, 140502(R) (2019).
- [12] C. Duan, K. Sasmal, M. B. Maple, A. Podlesnyak, J.-X. Zhu, Q. Si, and P. Dai, Incommensurate spin fluctuations in the spin-triplet superconductor candidate  $Ute_2$ , *Phys. Rev. Lett.* **125**, 237003 (2020).
- [13] W. Knafo, G. Knebel, P. Steffens, K. Kaneko, A. Rosuel, J.-P. Brison, J. Flouquet, D. Aoki, G. Lapertot, and S. Raymond, Low-dimensional antiferromagnetic fluctuations in the heavy-fermion paramagnetic ladder compound  $Ute_2$ , *Phys. Rev. B* **104**, L100409 (2021).
- [14] S. Raymond, W. Knafo, G. Knebel, K. Kaneko, J.-P. Brison, J. Flouquet, D. Aoki, and G. Lapertot, Feedback of superconductivity on the magnetic excitation spectrum of  $Ute_2$ , *J. Phys. Soc. Jpn.* **90**, 113706 (2021), <https://doi.org/10.7566/JPSJ.90.113706>.
- [15] K. Ishihara, M. Roppongi, M. Kobayashi, K. Imamura, Y. Mizukami, H. Sakai, P. Opletal, Y. Tokiwa, Y. Haga, K. Hashimoto, and T. Shibauchi, Chiral superconductivity in  $Ute_2$  probed by anisotropic low-energy excitations, *Nature Communications* **14**, 2966 (2023).
- [16] Y. Tokunaga, H. Sakai, S. Kambe, P. Opletal, Y. Tokiwa, Y. Haga, S. Kitagawa, K. Ishida, D. Aoki, G. Knebel, G. Lapertot, S. Krämer, and M. Horvatić, Longitudinal spin fluctuations driving field-reinforced superconductivity in  $Ute_2$ , *Phys. Rev. Lett.* **131**, 226503 (2023).
- [17] H. Matsumura, S. Kitagawa, S. Ogata, R. Matsubayashi, H. Fujibayashi, K. Kinjo, K. Ishida, Y. Tokunaga, H. Sakai, S. Kambe, A. Nakamura, Y. Shimizu, Y. Homma, D. Li, F. Honda, A. Miyake, and D. Aoki, Intrinsic low-temperature magnetic properties on ultraclean  $Ute_2$  with  $T_c = 2.1$ K revealed by  $^{125}\text{Te}$  nmr, *Phys. Rev. B* **111**, 094507 (2025).
- [18] D. Braithwaite, M. Vališka, G. Knebel, G. Lapertot, J.-P. Brison, A. Pourret, M. E. Zhitomirsky, J. Flouquet, F. Honda, and D. Aoki, Multiple superconducting phases in a nearly ferromagnetic system, *Communications Physics* **2**, 147 (2019).
- [19] S. Ran, H. Kim, I.-L. Liu, S. R. Saha, I. Hayes, T. Metz, Y. S. Eo, J. Paglione, and N. P. Butch, Enhancement and reentrance of spin triplet superconductivity in  $Ute_2$  under pressure, *Phys. Rev. B* **101**, 140503(R) (2020).
- [20] W.-C. Lin, D. J. Campbell, S. Ran, I.-L. Liu, H. Kim, A. H. Nevidomskyy, D. Graf, N. P. Butch, and J. Paglione, Tuning magnetic confinement of spin-triplet superconductivity, *npj Quantum Materials* **5**, 68 (2020).
- [21] G. Knebel, M. Kimata, M. Vališka, F. Honda, D. Li, D. Braithwaite, G. Lapertot, W. Knafo, A. Pourret, Y. J. Sato, Y. Shimizu, T. Kihara, J.-P. Brison, J. Flouquet, and D. Aoki, Anisotropy of the upper critical field in the heavy-fermion superconductor  $Ute_2$  under pressure, *J. Phys. Soc. Jpn.* **89**, 053707 (2020).
- [22] D. Aoki, F. Honda, G. Knebel, D. Braithwaite, A. Nakamura, D. Li, Y. Homma, Y. Shimizu, Y. J. Sato, J.-P. Brison, and J. Flouquet, Multiple superconducting phases and unusual enhancement of the upper critical field in  $Ute_2$ , *J. Phys. Soc. Jpn.* **89**, 053705 (2020).
- [23] K. Kinjo, H. Fujibayashi, S. Kitagawa, K. Ishida, Y. Tokunaga, H. Sakai, S. Kambe, A. Nakamura, Y. Shimizu, Y. Homma, D. X. Li, F. Honda, D. Aoki, K. Hiraki, M. Kimata, and T. Sasaki, Change of superconducting character in  $Ute_2$  induced by magnetic field, *Phys. Rev. B* **107**, L060502 (2023).
- [24] Y. Tokiwa, P. Opletal, H. Sakai, K. Kubo, E. Yamamoto, S. Kambe, M. Kimata, S. Awaji, T. Sasaki, D. Aoki, Y. Tokunaga, and Y. Haga, Stabilization of superconductivity by metamagnetism in an easy-axis magnetic field on  $U\text{Te}_2$ , *arXiv e-prints*, arXiv:2210.11769 (2022).
- [25] J. Ishizuka, S. Sumita, A. Daido, and Y. Yanase, Insulator-metal transition and topological superconductivity in  $Ute_2$  from a first-principles calculation, *Phys. Rev. Lett.* **123**, 217001 (2019).
- [26] L. Jiao, S. Howard, S. Ran, Z. Wang, J. O. Rodriguez, M. Sigrist, Z. Wang, N. P. Butch, and V. Madhavan, Chiral superconductivity in heavy-fermion metal  $Ute_2$ , *Nature* **579**, 523 (2020).
- [27] T. C. Wu, H. K. Pal, and M. S. Foster, Topological anomalous skin effect in weyl superconductors, *Phys. Rev. B* **103**, 104517 (2021).
- [28] Y. Yu, V. Madhavan, and S. Raghu, Majorana fermion arcs and the local density of states of  $Ute_2$ , *Phys. Rev. B* **105**, 174520 (2022).
- [29] D. Shaffer and D. V. Chichinadze, Chiral superconductivity in  $Ute_2$  via emergent  $C_4$  symmetry and spin-orbit coupling, *Phys. Rev. B* **106**, 014502 (2022).
- [30] J. Tei, T. Mizushima, and S. Fujimoto, Possible realization of topological crystalline superconductivity with time-reversal symmetry in  $Ute_2$ , *Phys. Rev. B* **107**, 144517 (2023).
- [31] X.-L. Qi and S.-C. Zhang, Topological insulators and superconductors, *Rev. Mod. Phys.* **83**, 1057 (2011).
- [32] M. Sato and S. Fujimoto, Majorana fermions and topology in superconductors, *J. Phys. Soc. Jpn.* **85**, 072001 (2016).
- [33] M. Sato and Y. Ando, Topological superconductors: a review, *Rep. Prog. Phys.* **80**, 076501 (2017).
- [34] G. Nakamine, S. Kitagawa, K. Ishida, Y. Tokunaga, H. Sakai, S. Kambe, A. Nakamura, Y. Shimizu, Y. Homma, D. Li, F. Honda, and D. Aoki, Superconducting properties of heavy fermion  $Ute_2$  revealed by 125Te-nuclear magnetic resonance, *J. Phys. Soc. Jpn.* **88**, 113703 (2019).
- [35] G. Nakamine, K. Kinjo, S. Kitagawa, K. Ishida, Y. Tokunaga, H. Sakai, S. Kambe, A. Nakamura, Y. Shimizu, Y. Homma, D. Li, F. Honda, and D. Aoki, Anisotropic response of spin susceptibility in the superconducting state of  $Ute_2$  probed with  $^{125}\text{Te}$ -NMR measurement, *Phys. Rev. B* **103**, L100503 (2021).
- [36] G. Nakamine, K. Kinjo, S. Kitagawa, K. Ishida, Y. Tokunaga, H. Sakai, S. Kambe, A. Nakamura, Y. Shimizu, Y. Homma, D. Li, F. Honda, and D. Aoki, Inhomogeneous superconducting

- state probed by 125te nmr on ute2, *J. Phys. Soc. Jpn.* **90**, 064709 (2021), <https://doi.org/10.7566/JPSJ.90.064709>.
- [37] H. Fujibayashi, G. Nakamine, K. Kinjo, S. Kitagawa, K. Ishida, Y. Tokunaga, H. Sakai, S. Kambe, A. Nakamura, Y. Shimizu, Y. Homma, D. Li, F. Honda, and D. Aoki, Superconducting order parameter in ute2 determined by knight shift measurement, *J. Phys. Soc. Jpn.* **91**, 043705 (2022), <https://doi.org/10.7566/JPSJ.91.043705>.
- [38] H. Matsumura, H. Fujibayashi, K. Kinjo, S. Kitagawa, K. Ishida, Y. Tokunaga, H. Sakai, S. Kambe, A. Nakamura, Y. Shimizu, Y. Homma, D. Li, F. Honda, and D. Aoki, Large reduction in the a-axis knight shift on ute2 with  $t_c = 2.1$  k, *J. Phys. Soc. Jpn.* **92**, 063701 (2023), <https://doi.org/10.7566/JPSJ.92.063701>.
- [39] S. Kitagawa, K. Nakanishi, H. Matsumura, Y. Takahashi, K. Ishida, Y. Tokunaga, H. Sakai, S. Kambe, A. Nakamura, Y. Shimizu, Y. Homma, D. Li, F. Honda, A. Miyake, and D. Aoki, Clear reduction in spin susceptibility and superconducting spin rotation for  $h \parallel a$  in the early-stage sample of spin-triplet superconductor ute2, *J. Phys. Soc. Jpn.* **93**, 123701 (2024), <https://doi.org/10.7566/JPSJ.93.123701>.
- [40] I. M. Hayes, D. S. Wei, T. Metz, J. Zhang, Y. S. Eo, S. Ran, S. R. Saha, J. Collini, N. P. Butch, D. F. Agterberg, A. Kapitulnik, and J. Paglione, Multicomponent superconducting order parameter in ute2, *Science* **373**, 797 (2021), <https://www.science.org/doi/pdf/10.1126/science.abb0272>.
- [41] D. S. Wei, D. Saykin, O. Y. Miller, S. Ran, S. R. Saha, D. F. Agterberg, J. Schmalian, N. P. Butch, J. Paglione, and A. Kapitulnik, Interplay between magnetism and superconductivity in ute2, *Phys. Rev. B* **105**, 024521 (2022).
- [42] M. O. Ajeesh, M. Bordelon, C. Girod, S. Mishra, F. Ronning, E. D. Bauer, B. Maiorov, J. D. Thompson, P. F. S. Rosa, and S. M. Thomas, Fate of time-reversal symmetry breaking in ute2, *Phys. Rev. X* **13**, 041019 (2023).
- [43] S. Wang, K. Zhussupbekov, J. P. Carroll, B. Hu, X. Liu, E. Pangburn, A. Crepieux, C. Pepin, C. Broyles, S. Ran, N. P. Butch, S. Saha, J. Paglione, C. Bena, J. C. Séamu Davis, and Q. Gu, Imaging Odd-Parity Quasiparticle Interference in the Superconductive Surface State of UTe2, *arXiv e-prints*, [arXiv:2503.17761](https://arxiv.org/abs/2503.17761) (2025).
- [44] N. Sharma, M. Toole, J. McKenzie, F. Cheng, S. M. Thomas, P. F. S. Rosa, Y.-T. Hsu, and X. Liu, Observation of Persistent Zero Modes and Superconducting Vortex Doublets in UTe2, *arXiv e-prints*, [arXiv:2503.17450](https://arxiv.org/abs/2503.17450) (2025).
- [45] A. B. Shick and W. E. Pickett, Spin-orbit coupling induced degeneracy in the anisotropic unconventional superconductor ute2, *Phys. Rev. B* **100**, 134502 (2019).
- [46] Y. Xu, Y. Sheng, and Y. feng Yang, Quasi-two-dimensional fermi surfaces and unitary spin-triplet pairing in the heavy fermion superconductor ute2, *Phys. Rev. Lett.* **123**, 217002 (2019).
- [47] T. Shishidou, H. G. Suh, P. M. R. Brydon, M. Weinert, and D. F. Agterberg, Topological band and superconductivity in ute2, *Phys. Rev. B* **103**, 104504 (2021).
- [48] K. Hiranuma and S. Fujimoto, Paramagnetic effects of j-electron superconductivity and application to ute2, *J. Phys. Soc. Jpn.* **90**, 034707 (2021).
- [49] J. Ishizuka and Y. Yanase, Periodic anderson model for magnetism and superconductivity in ute2, *Phys. Rev. B* **103**, 094504 (2021).
- [50] Y. Moriya, T. Matsushita, M. G. Yamada, T. Mizushima, and S. Fujimoto, Intrinsic anomalous thermal hall effect in the unconventional superconductor ute2, *J. Phys. Soc. Jpn.* **91**, 094710 (2022).
- [51] A. Kreisel, Y. Quan, and P. J. Hirschfeld, Spin-triplet superconductivity driven by finite-momentum spin fluctuations, *Phys. Rev. B* **105**, 104507 (2022).
- [52] S. Kanasugi and Y. Yanase, Anapole superconductivity from pt-symmetric mixed-parity interband pairing, *Commun. Phys.* **5**, 39 (2022).
- [53] M. Chazono, S. Kanasugi, T. Kitamura, and Y. Yanase, Piezoelectric effect and diode effect in anapole and monopole superconductors, *Phys. Rev. B* **107**, 214512 (2023).
- [54] T. Kitamura, S. Kanasugi, M. Chazono, and Y. Yanase, Quantum geometry induced anapole superconductivity, *Phys. Rev. B* **107**, 214513 (2023).
- [55] A. Rosuel, C. Marcenat, G. Knebel, T. Klein, A. Pourret, N. Marquardt, Q. Niu, S. Rousseau, A. Demuer, G. Seyfarth, G. Lapertot, D. Aoki, D. Braithwaite, J. Flouquet, and J. P. Brison, Field-induced tuning of the pairing state in a superconductor, *Phys. Rev. X* **13**, 011022 (2023).
- [56] F. Theuss, A. Shragai, G. Grissonnanche, I. M. Hayes, S. R. Saha, Y. S. Eo, A. Suarez, T. Shishidou, N. P. Butch, J. Paglione, and B. J. Ramshaw, Single-component superconductivity in ute2 at ambient pressure, *Nature Physics* **20**, 1124 (2024).
- [57] T. Hazra and P. A. Volkov, Pair kondo effect: A mechanism for time-reversal symmetry breaking superconductivity in ute2, *Phys. Rev. B* **109**, 184501 (2024).
- [58] R. Hakuno, K. Nogaki, and Y. Yanase, Magnetism and superconductivity in mixed-dimensional periodic anderson model for ute2, *Phys. Rev. B* **109**, 104509 (2024).
- [59] L. Zhang, C. Guo, D. Graf, C. Putzke, M. M. Bordelon, E. D. Bauer, S. M. Thomas, F. Ronning, P. F. S. Rosa, and P. J. W. Moll, Dimensionality of the reinforced superconductivity in ute2, *Nature Communications* **16**, 10308 (2025).
- [60] R. Hakuno and Y. Yanase, Superconductivity in ute2 from local noncentrosymmetry (2025), [arXiv:2510.14259](https://arxiv.org/abs/2510.14259) [cond-mat.supr-con].
- [61] M. Shimizu and Y. Yanase, Magnetic fluctuations and anisotropy in ute2: a multi-orbital study based on gga+u and rpa (2025), [arXiv:2510.15322](https://arxiv.org/abs/2510.15322) [cond-mat.str-el].
- [62] I. M. Hayes, E. Fang, S. R. Saha, V. Mishra, P. J. Hirschfeld, and J. Paglione, Field-angle-resolved heat transport in ute2: determination of nodal positions in the superconducting order parameter (2025), [arXiv:2512.13877](https://arxiv.org/abs/2512.13877) [cond-mat.supr-con].
- [63] K. Totsuka, Y. Kono, Y. Shimizu, A. Nakamura, A. Miyake, D. Aoki, Y. Tsutsumi, K. Machida, and S. Kittaka, Nodal superconductivity of ute2 probed by field-angle-resolved specific heat on a crystal with  $t_c = 2.1$  k (2026), [arXiv:2601.08201](https://arxiv.org/abs/2601.08201) [cond-mat.supr-con].
- [64] S.-i. Fujimori, I. Kawasaki, Y. Takeda, H. Yamagami, A. Nakamura, Y. Homma, and D. Aoki, Electronic structure of ute2 studied by photoelectron spectroscopy, *J. Phys. Soc. Jpn.* **88**, 103701 (2019).
- [65] L. Miao, S. Liu, Y. Xu, E. C. Kotta, C.-J. Kang, S. Ran, J. Paglione, G. Kotliar, N. P. Butch, J. D. Denlinger, and L. A. Wray, Low energy band structure and symmetries of ute2 from angle-resolved photoemission spectroscopy, *Phys. Rev. Lett.* **124**, 076401 (2020).
- [66] Q. Niu, G. Knebel, D. Braithwaite, D. Aoki, G. Lapertot, G. Seyfarth, J.-P. Brison, J. Flouquet, and A. Pourret, Fermi-surface instability in the heavy-fermion superconductor ute2, *Phys. Rev. Lett.* **124**, 086601 (2020).
- [67] D. Aoki, H. Sakai, P. Opletal, Y. Tokiwa, J. Ishizuka, Y. Yanase, H. Harima, A. Nakamura, D. Li, Y. Homma, Y. Shimizu, G. Knebel, J. Flouquet, and Y. Haga, First observation of the de haas-van alphen effect and fermi surfaces in the unconventional superconductor ute2, *J. Phys. Soc. Jpn.* **91**, 083704 (2022).

- (2022), <https://doi.org/10.7566/JPSJ.91.083704>.
- [68] D. Aoki, I. Sheikin, A. McCollam, J. Ishizuka, Y. Yanase, G. Lapertot, J. Flouquet, and G. Knebel, de haas–van alphen oscillations for the field along c-axis in  $ut_2$ , *J. Phys. Soc. Jpn* **92**, 065002 (2023), <https://doi.org/10.7566/JPSJ.92.065002>.
- [69] C. Broyles, Z. Rehfuss, H. Siddiquee, J. A. Zhu, K. Zheng, M. Nikolo, D. Graf, J. Singleton, and S. Ran, Revealing a 3d fermi surface pocket and electron-hole tunneling in  $ut_2$  with quantum oscillations, *Phys. Rev. Lett.* **131**, 036501 (2023).
- [70] A. G. Eaton, T. I. Weinberger, N. J. M. Popiel, Z. Wu, A. J. Hickey, A. Cabala, J. Pospíšil, J. Prokleška, T. Haidamak, G. Bastien, P. Opletal, H. Sakai, Y. Haga, R. Nowell, S. M. Benjamin, V. Sechovský, G. G. Lonzarich, F. M. Grosche, and M. Vališka, Quasi-2d fermi surface in the anomalous superconductor  $ut_2$ , *Nature Communications* **15**, 223 (2024).
- [71] H. Sakai, P. Opletal, Y. Tokiwa, E. Yamamoto, Y. Tokunaga, S. Kambe, and Y. Haga, Single crystal growth of superconducting  $ut_2$  by molten salt flux method, *Phys. Rev. Mater.* **6**, 073401 (2022).
- [72] D. Aoki, Molten salt flux liquid transport method for ultra clean single crystals  $ut_2$ , *J. Phys. Soc. Jpn.* **93**, 043703 (2024), <https://doi.org/10.7566/JPSJ.93.043703>.
- [73] Y. S. Eo, S. Liu, S. R. Saha, H. Kim, S. Ran, J. A. Horn, H. Hodovanets, J. Collini, T. Metz, W. T. Fuhrman, A. H. Nevidomskyy, J. D. Denlinger, N. P. Butch, M. S. Fuhrer, L. A. Wray, and J. Paglione, c-axis transport in  $ut_2$ : Evidence of three-dimensional conductivity component, *Phys. Rev. B* **106**, L060505 (2022).
- [74] H. C. Choi, S. H. Lee, and B.-J. Yang, Correlated normal state fermiology and topological superconductivity in  $UTe_2$ , *Communications Physics* **7**, 273 (2024).
- [75] B. Kang, M.-H. Kim, and C. H. Park, Coexistence of 3D and quasi-2D Fermi surfaces driven by orbital selective Kondo scattering in  $UTe_2$ , *arXiv e-prints*, [arXiv:2502.03646](https://arxiv.org/abs/2502.03646) (2025).
- [76] D. Aoki, I. Sheikin, N. Marquardt, G. Lapertot, J. Flouquet, and G. Knebel, High field superconducting phases of ultra clean single crystal  $ut_2$ , *J. Phys. Soc. Jpn.* **93**, 123702 (2024), <https://doi.org/10.7566/JPSJ.93.123702>.
- [77] T. I. Weinberger, Z. Wu, D. E. Graf, Y. Skourski, A. Cabala, J. Pospíšil, J. Prokleška, T. Haidamak, G. Bastien, V. Sechovský, G. G. Lonzarich, M. Vališka, F. M. Grosche, and A. G. Eaton, Quantum interference between quasi-2d fermi surface sheets in  $ut_2$ , *Phys. Rev. Lett.* **132**, 266503 (2024).
- [78] F. Husstedt, M. Kimata, S. Naduvile Thadathil, B. Valentin Schwarze, M. König, G. Lapertot, J.-P. Brison, G. Knebel, D. Aoki, J. Wosnitza, and T. Helm, Slow magnetic quantum oscillations in the c-axis magnetoresistance of  $UTe_2$ , *arXiv e-prints*, [arXiv:2503.11525](https://arxiv.org/abs/2503.11525) (2025).
- [79] K. Yamaji, On the angle dependence of the magnetoresistance in quasi-two-dimensional organic superconductors, *J. Phys. Soc. Jpn.* **58**, 1520 (1989), <https://doi.org/10.1143/JPSJ.58.1520>.
- [80] S. K. Lewin and J. G. Analytis, Angle-dependent magnetoresistance as a probe of fermi surface warping in  $HgBa_2CuO_{4+\delta}$ , *Phys. Rev. B* **98**, 075116 (2018).
- [81] S. Zhang, Q. Wu, Y. Liu, and O. V. Yazyev, Magnetoresistance from fermi surface topology, *Phys. Rev. B* **99**, 035142 (2019).
- [82] M. Kimata, T. Helm, H. Shimizu, A. Nakamura, D. Li, Y. Honma, A. Miyake, D. Aoki, The Physical Society of Japan 2024 Annual (79th) Meeting.
- [83] P. Blaha, K. Schwarz, G. K. H. Madsen, D. Kvasnicka, J. Luitz, R. Laskowski, F. Tran, and L. D. Marks, *WIEN2k, An Augmented Plane Wave + Local Orbitals Program for Calculating Crystal Properties* (Karlheinz Schwarz, Techn. Universität Wien, Austria, 2018).
- [84] G. Pizzi, V. Vitale, R. Arita, S. Blügel, F. Freimuth, G. Géranton, M. Gibertini, D. Gresch, C. Johnson, T. Koretsune, J. Ibañez-Azpiroz, H. Lee, J.-M. Lihm, D. Marchand, A. Marrazzo, Y. Mokrousov, J. I. Mustafa, Y. Nohara, Y. Nomura, L. Paulatto, S. Poncé, T. Ponweiser, J. Qiao, F. Thöle, S. S. Tsirkin, M. Wierzbowska, N. Marzari, D. Vanderbilt, I. Souza, A. A. Mostofi, and J. R. Yates, Wannier90 as a community code: new features and applications, *Journal of Physics: Condensed Matter* **32**, 165902 (2020).
- [85] J. Kuneš, R. Arita, P. Wissgott, A. Toschi, H. Ikeda, and K. Held, Wien2wannier: From linearized augmented plane waves to maximally localized wannier functions, *Computer Physics Communications* **181**, 1888 (2010).
- [86] Q. Wu, S. Zhang, H.-F. Song, M. Troyer, and A. A. Soluyanov, Wanniertools: An open-source software package for novel topological materials, *Computer Physics Communications* **224**, 405 (2018).
- [87] N. W. Ashcroft and N. D. Mermin, *Solid state physics*, harcourt, Orlando, 1976.
- [88] K. Momma and F. Izumi, VESTA3 for three-dimensional visualization of crystal, volumetric and morphology data, *Journal of Applied Crystallography* **44**, 1272 (2011).
- [89] M. Kawamura, Fermisurfer: Fermi-surface viewer providing multiple representation schemes, *Computer Physics Communications* **239**, 197 (2019).